NANO LETTERS

Letter

pubs.acs.org/NanoLett

Designed Quasi-1D Potential Structures Realized in Compositionally Graded $InAs_{1-x}P_x$ Nanowires

Gustav Nylund,[†] Kristian Storm,[†] Sebastian Lehmann,[†] Federico Capasso,[‡] and Lars Samuelson*[,†]

[†]Division of Solid State Physics and NanoLund, Lund University, P.O. Box 118, 221 00 Lund, Sweden

[‡]School of Engineering and Applied Sciences, Harvard University, Cambridge, Massachusetts 02138, United States

Supporting Information

ABSTRACT: III−V semiconductor heterostructures are important components of many solid-state optoelectronic devices, but the ability to control and tune the electrical and optical properties of these structures in conventional device geometries is fundamentally limited by the bulk dimensionality and the inability to accommodate lattice-mismatched material combinations. Here we demonstrate how semiconductor nanowires may enable the creation of arbitrarily shaped one-dimensional potential structures for new types of designed device functionality. We describe the controlled growth of stepwise compositionally graded $InAs_{1-x}P_x$ heterostructures defined along the axes of InAs nanowires, and we show that nanowires with sawtooth-shaped composition profiles behave as near-ideal unipolar diodes with ratchet-like rectification of the electron transport through the nanowires, in excellent agreement with simulations. This new type of designed quasi-1D potential structure represents a significant advance in band gap engineering and may enable fundamental studies of low-dimensional hot-carrier dynamics, in addition to constituting a platform for implementing novel electronic and optoelectronic device concepts.

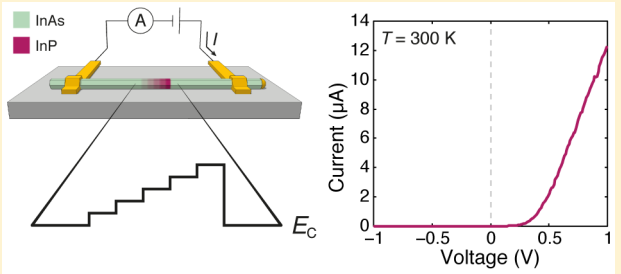

KEYWORDS: *Semiconductor nanowire, heterostructure, band gap engineering, InAs, InP, chemical beam epitaxy*

Semiconductor heterostructures are key building blocks for many important solid-state device technologies and have enabled the development of semiconductor lasers,[1,2] high-electron-mobility transistors,[3] resonant-tunneling diodes,[4] and heterojunction bipolar transistors.[5] By combining semiconductor materials with different band gaps or modulating the composition of compound semiconductor alloys—a process known as band gap engineering[6]—it is possible to design materials with customized optical and electrical properties, tailored to specific device applications. The ability to design and create structures in which the electric potential is of arbitrary complexity is a long-term dream in electronics and photonics. Until now, such systems have primarily been realized in 3D structures, with a designed potential in only one dimension, say z. In these structures, the charge carriers remain unconstrained in the x and y dimensions, which drastically reduces the degree to which they may be controlled. To achieve optimal control, it is necessary to structure the system in all three dimensions, and one way of achieving this is to reduce its physical dimensionality. Semiconductor nanowires are promising candidates for this approach because of their quasi-1D geometry, which provides both lateral confinement of charge carriers and a highly efficient strain relaxation mechanism, enabling defect-free formation of lattice-mismatched heterostructures along the nanowire axis.[7−9]

Axial nanowire heterostructures were first grown more than a decade ago[10−12] but have until now mainly been used to create abrupt heterostructures and thin tunnel barriers for various types of quantum devices, such as single-electron transistors[13] and resonant-tunneling diodes[14] (Figure 1a). In this paper, we demonstrate how semiconductor nanowires may allow the creation of continuous (or stepwise varying), axially graded heterostructures through highly controlled in situ modulation of the chemical composition along the nanowire axis. Earlier studies have shown that chemical beam epitaxy (CBE) is capable of producing axial InAs/InP nanowire heterojunctions with atomically sharp interfaces,[10] as well as $InAs/InAs_{1-x}P_x$ heterostructures spanning the entire composition range.[15,16] Here, we have further developed this growth technique so that we are able to grow designed axial potential structures via compositional grading in a controlled manner. This is done using heterostructure sequences consisting of an arbitrary number of $InAs_{1-x}P_x$ segments of any length and composition. We have demonstrated this capability by making two types of designed potential structures: (i) an asymmetric, sawtooth-shaped potential and (ii) a symmetric, pyramid-shaped potential (Figure 1b). We have used the asymmetric structure to create a unipolar nanowire diode in which the spatial asymmetry of the sawtooth-shaped potential leads to ratchet-like rectification of electron transport through the nanowire. The shape of the current-rectifying potential is determined directly by the grading of the chemical composition, rather than

Received: October 6, 2015
Revised: January 14, 2016
Published: January 20, 2016

DOI: 10.1021/acs.nanolett.5b04067
Nano Lett. 2016, 16, 1017−1021

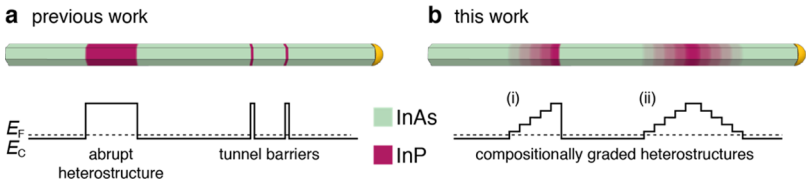

Figure 1. Axial nanowire heterostructures. (a) Previous work has demonstrated growth of axial heterostructures with abrupt transitions, primarily for the purpose of creating thin tunnel barriers for use in quantum transport devices. (b) In this work, we have developed a technique for growing stepwise compositionally graded heterostructures along the nanowire axis that allows us to design and create quasi-1D potential profiles of nearly arbitrary shape and size, here demonstrated by sawtooth-shaped (i) and pyramid-shaped (ii) composition profiles.

by impurity doping (p−n junctions) or metal−semiconductor junctions (Schottky barriers), offering a higher degree of tunability in terms of the height, width, and shape of the potential. This particular sawtooth-shaped potential structure is highly interesting for fundamental studies of low-dimensional hot-carrier dynamics and ratchet physics in the solid state, as well as for realizing novel optoelectronic device concepts. However, it is important to note that, in principle, our growth technique is capable of making any arbitrarily shaped one-dimensional potential profile through a simple discretization approach in which the desired composition profile is divided into short segments of constant composition.

InAs nanowires with stepwise compositionally graded $InAs_{1-x}P_x$ segments were grown by CBE on an epiready InAs(111)B substrate. Nanowire growth was catalytically promoted by Au aerosol particles[17] approximately 40 nm in diameter, resulting in nanowires with a diameter of 50 ± 5 nm and a length of approximately 2.2 μm. The chemical composition of the nanowires was modulated during growth by sequentially switching off the Group-III supply (TMIn), thus temporarily interrupting nanowire growth by terminating the flow of In to the seed particle, and adjusting the Group-V flow rates (TBAs, TBP). Nanowire growth was resumed when the Group-III source was switched back on, with a ternary composition determined by the TBAs/TBP ratio. In this way, by frequently interrupting nanowire growth and retuning the Group-V precursor ratio, it is possible to achieve a stepwise, quasi-graded transition from InAs to InP consisting of any number of ternary $InAs_{1-x}P_x$ steps of arbitrary composition x. For this particular study, the phosphorus content was ramped up in five stages over a distance of around 200 nm. To form nanowires with a symmetrical variation in potential, the phosphorus content was gradually ramped back down, resulting in a pyramid-shaped composition profile. For the asymmetric nanowires, the phosphorus source was abruptly switched off after $InAs_{1-x}P_x$ segment growth, resulting in a sawtooth-shaped composition profile.

The crystal structure and chemical composition of the nanowires were characterized by high-resolution transmission electron microscopy (HRTEM), scanning transmission electron microscopy high-angle annular dark-field imaging (STEM−HAADF), and energy-dispersive X-ray spectroscopy (STEM−EDX). Please see Supporting Information for a detailed analysis of the nanowire crystal structure. Figure 2a shows a STEM−HAADF image of an InAs/$InAs_{1-x}P_x$/InAs nanowire with a sawtooth-shaped composition profile, and Figure 2b shows a close-up of the compositionally graded segment. In both figures, the stepwise increase in the phosphorus content can be seen as an incremental decrease in image contrast along the nanowire axis. An EDX line scan acquired along the length of the $InAs_{1-x}P_x$ segment (Figure 2c)

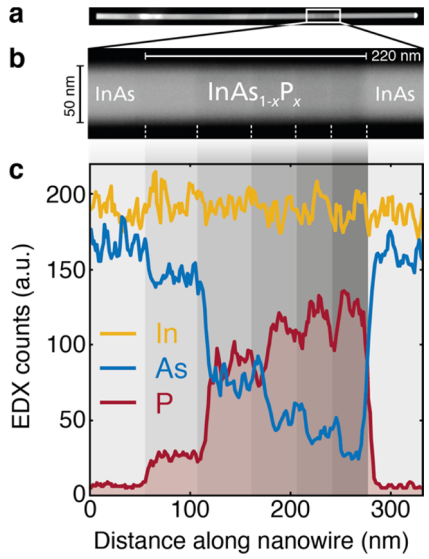

Figure 2. Composition profile of an asymmetrically graded InAs/$InAs_{1-x}P_x$/InAs nanowire. (a,b) STEM−HAADF images showing the sawtooth-shaped composition profile of the $InAs_{1-x}P_x$ segment (decreasing image contrast indicates higher P content). (c) EDX line scan along the $InAs_{1-x}P_x$ segment, showing stepwise increasing P content (red), stepwise decreasing As content (blue), and constant In content (yellow).

clearly shows five discrete steps of different ternary composition, with each step slightly more phosphorus-rich than the previous one. Quantitative analysis of the composition of the individual steps averaged over several different nanowires yields a slight spread in composition. At the top of the sawtooth, we find a peak phosphorus content in the range x = 0.8−0.9, corresponding to a conduction band offset of approximately 0.5−0.6 eV.[15]

After growth, the nanowires were broken off from the growth substrate and transferred to an insulating substrate for fabrication of Ohmic contacts, allowing us to perform two-terminal transport measurements to evaluate the effect of the composition profile symmetry on the electrical conductivity. A schematic illustration of the device design is shown in Figure 3a.

Figure 3b shows a simplified energy band diagram of a nanowire with a sawtooth-shaped composition profile at thermal equilibrium. Although the nanowires are nominally undoped, the InAs leads are degenerately n-type due to a combination of unintentional, in situ-incorporated carbon impurities acting as donors[18] and charge carrier accumulation from surface-state-induced band bending.[19] As a result, the Fermi level is expected to be pinned approximately 0.1 eV above the conduction band minimum.[20] Under the influence of

DOI: 10.1021/acs.nanolett.5b04067
Nano Lett. 2016, 16, 1017−1021

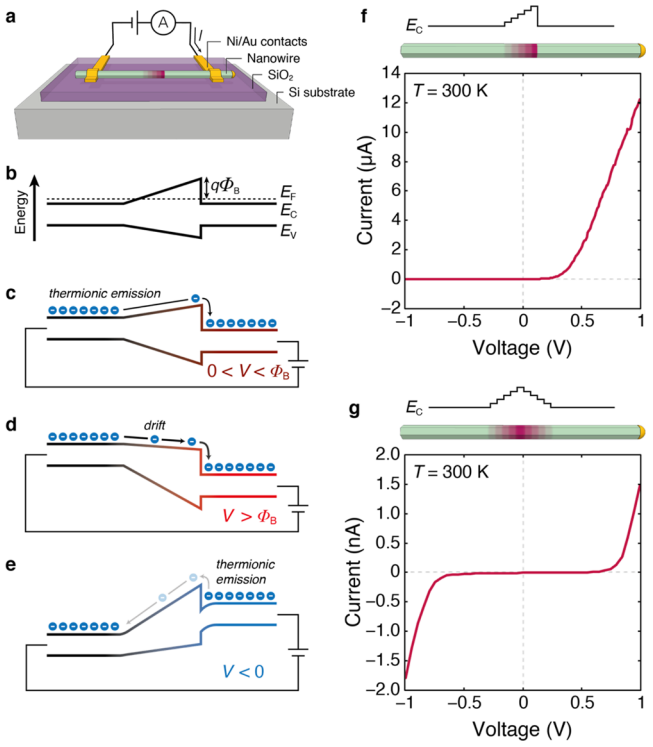

Figure 3. Symmetry-dependent current rectification in compositionally graded nanowires. (a) Schematic illustration of the two-terminal nanowire device used for measuring $I-V$ characteristics of compositionally graded nanowires. (b) Energy band diagram of InAs/$InAs_{1-x}P_x$/InAs nanowire with sawtooth-shaped composition profile at thermal equilibrium. A smoothly graded composition is shown for the sake of simplicity. (c–e) Energy band diagram under moderate (c) and strong (d) forward bias and under reverse bias (e), illustrating the ratchet-like rectification mechanism of the sawtooth-shaped potential. (f,g) Experimental $I-V$ characteristics recorded at room temperature for nanowires with asymmetric (f) and symmetric (g) quasi-graded composition profiles, showing a strongly symmetry-dependent electrical conductivity.

a bias voltage, the spatial asymmetry of the electric potential allows electrons to drift from the bottom of the nanowire to the top, but not in the opposite direction. At small forward bias (Figure 3c), electrons are injected by thermionic emission. Here, "small" implies that the applied electric field is smaller than the built-in quasi-electric field of the sawtooth-shaped barrier, i.e., that the applied voltage is less than the barrier height Φ_B. At higher forward bias (Figure 3d), the voltage drop across the graded segment generates an electric field that is larger than the built-in field, effectively eliminating the transport barrier. This leads to strong injection, in which electrons can drift across the graded segment from left to right (bottom to top of the nanowire), resulting in a large current. At reverse bias (Figure 3e), electron injection from right to left (top to bottom of the nanowire) is only possible through thermionic emission over the potential barrier or by thermionically assisted tunneling through the barrier (with the applied voltage modifying the effective barrier width), resulting in a much smaller current.

Figure 3f,g shows experimental $I-V$ characteristics recorded at room temperature for both a nanowire with an asymmetric, sawtooth-shaped composition profile and a nanowire with a symmetric, pyramid-shaped composition profile. As expected, the asymmetric nanowire exhibits a strongly asymmetric electrical conductivity with diode-like current rectification and a threshold voltage of approximately 0.4 V (Figure 3f). The symmetric nanowire exhibits a symmetric electrical conductivity, as well as a higher threshold voltage of approximately 0.8 V (Figure 3g). We expect the symmetric nanowire to have a higher threshold voltage because the length of the compositionally graded $InAs_{1-x}P_x$ segment over which most of the bias voltage is dropped (see below) is twice as long in the symmetric nanowires.

Temperature-dependent transport measurements were used to investigate further the thermionic emission of electrons across the sawtooth-shaped potential and to determine the barrier height Φ_B. Figure 4a,b shows experimental and

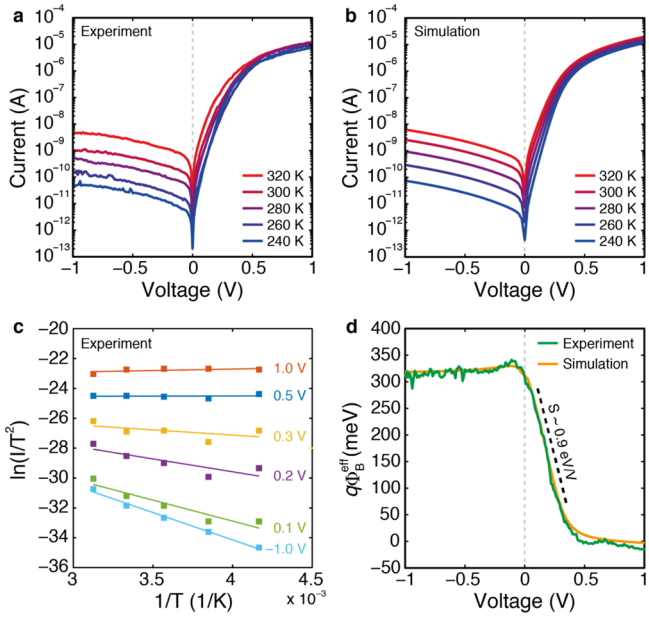

Figure 4. Electrical characterization of an InAs nanowire with an asymmetric, sawtooth-shaped composition profile. (a) Experimental and (b) simulated $I-V$ characteristics at different temperatures. (c) $\ln(I/T^2)$ as a function of $1/T$ for six different bias voltages. The solid lines are least-squares fits, where the slope of each line gives the effective barrier height at that bias voltage using eq 1 and eq 2. (d) Effective (voltage-dependent) barrier height extracted from experimental and simulated $I-V$ data.

simulated $I-V$ characteristics (see Methods for a description of the simulations) at a range of different temperatures plotted on a logarithmic current scale. As the temperature is decreased from 320 to 240 K, the reverse current (at negative bias voltages) drops by 2 orders of magnitude, while the forward current (at positive bias voltages) is affected only weakly. In reverse bias, the current through the nanowire is primarily limited by thermal injection of charge carriers over the potential barrier formed by the conduction band discontinuity, resulting in a current which is strongly temperature-dependent but only weakly voltage-dependent. The observed voltage dependence at reverse bias is slightly stronger than expected, which is most likely a result of carrier accumulation at the conduction band discontinuity, leading to band bending and a lowering of the effective barrier height. At small forward bias, the voltage drop across the quasi-graded nanowire segment also lowers the effective height of the barrier, resulting in a temperature-dependent current caused by thermally activated carrier injection. At large forward bias, the barrier is completely

DOI: 10.1021/acs.nanolett.5b04067
Nano Lett. 2016, 16, 1017–1021

eliminated by the voltage drop across it, and the current is instead limited by contact resistance and the series resistances of the InAs leads, resulting in a strongly voltage-dependent current with only a weak temperature dependence.

For moderate forward and reverse bias, when thermionic emission is the dominating carrier injection mechanism, the current I across the barrier for a given voltage bias V and temperature T can be described by the Shockley diode equation

$$I = I_0\left[\exp\left(\frac{qV}{nkT}\right) - 1\right] \quad (1)$$

where q is the elementary charge; n is an ideality factor (equal to unity for an ideal diode); and k is Boltzmann's constant, and with the reverse saturation current I_0 given by

$$I_0 = AA^*T^2 \exp\left(-\frac{q\Phi_B}{kT}\right) \quad (2)$$

where A is the cross-sectional area of the nanowire; A^* is the effective Richardson constant; and the activation energy $q\Phi_B$ is the height of the sawtooth-shaped barrier, i.e., the energy difference between the Fermi level in the InAs leads and the conduction band edge at the top of the barrier.

While the barrier height $q\Phi_B$ is technically a voltage-independent parameter, an effective barrier height for different values of applied bias can still be extracted from both experimental and simulated $I-V$ data by replacing $q\Phi_B$ in eq 2 with a voltage-dependent barrier height $q\Phi_B^{eff}(V)$ and analyzing how the current through the nanowire changes with temperature. To illustrate this, Figure 4c shows experimental $I-V$ data plotted as $\ln(I/T^2)$ versus $1/T$ for six representative bias voltages. The lines are linear least-squares fits to the data points, where the slope of each line gives the effective barrier height $q\Phi_B^{eff}$ at that voltage bias according to eq 1 and eq 2. Figure 4d shows the effective barrier height extracted in this way as a function of applied bias voltage, which is in excellent agreement with simulations. An extrapolation to zero bias yields a barrier height $q\Phi_B$ of 0.33 eV, which corresponds quite well with the predicted conduction band offset of 0.5 eV, considering that the Fermi level is expected to be pinned more than 0.1 eV above the conduction band minimum, as discussed previously. The difference is most likely due to field- and thermally assisted tunneling processes, both of which are not accounted for in eq 1 and eq 2, which will cause the extracted barrier height to slightly underestimate the actual barrier height. At small forward bias, we observe that the effective barrier height decreases linearly with applied bias at a rate of 0.9 eV/V, indicating that most of the voltage drops across the quasi-graded segment. At large forward bias, the transport barrier is completely eliminated by the voltage drop across it, and the effective barrier height goes to zero. At reverse bias, the effective barrier height decreases slightly with applied bias, which we attribute to the band bending induced by carrier accumulation mentioned previously.

In conclusion, we have demonstrated a realization of designed quasi-1D potential profiles using controlled modulation of the chemical composition along the axes of InAs/$InAs_{1-x}P_x$ nanowires. Nanowires with asymmetric, sawtooth-shaped composition profiles behave as near-ideal majority-carrier diodes, in which the height and shape of the current-rectifying potential is directly encoded in the quasi-graded chemical composition of the nanowire. To the best of the authors' knowledge, this is the first report of intentional, controlled growth of compositionally graded III−V nanowires for designed device functionality. These types of designed quasi-1D potential structures are highly interesting for fundamental studies of hot-carrier transport in low-dimensional semiconductor systems, for which the compositionally graded sawtooth potential can be used as a quasi-1D launch ramp for hot-electron spectroscopy.[21] By growing nanowires with several sawtooth-shaped potential structures in series, one could also create a periodic, solid-state ratchet potential. Such a structure might find technical applications as a staircase avalanche photodiode for low-noise optical detection, as first proposed by Williams, Capasso, and Tsang: if the material composition is chosen so that the conduction band step is greater than the electron ionization energy in the low-band gap material immediately following the step, a single photogenerated electron could generate a very large photocurrent through a series of cascaded impact ionization events, mimicking the functionality of a photomultiplier, but with an intrinsically higher signal-to-noise ratio due to the deterministic nature of the sawtooth-assisted avalanche multiplication.[22]

Methods. *Nanowire Growth.* Nanowires were grown using Au aerosol particles on an InAs(111)B substrate in a chemical beam epitaxy (CBE) system. The precursors for In, As, and P were trimethylindium (TMIn), precracked tertiarybutylarsine (TBAs), and precracked tertiarybutylphosphine (TBP), respectively. Prior to growth, the substrate was annealed under As pressure at 520 °C to remove any surface oxide. The temperature was then lowered to 400 °C, and a flow of In was introduced into the chamber. The source pressures were measured in the lines prior to entering the growth chamber. The growth was done in seven sequential steps. First, an InAs stem was grown using 1.5 mbar TBAs and 0.1 mbar TMIn. During gas type or pressure switching, the flow of TMIn to the chamber was stopped, interrupting nanowire growth. The growth interruption time was determined by the time required for the PID controllers to reach stable pressures in the gas lines, which was approximately 30 s. The five $InAs_{1-x}P_x$ segments were grown using a constant TMIn pressure of 0.1 mbar and a constant TBP pressure of 1 mbar, while the TBAs pressure was varied. The TBAs pressures in the five segments were 0.5, 0.3, 0.2, 0.12, and 0.08 mbar. A final contact segment was then grown using only TMIn and TBAs at 0.1 and 1.5 mbar, respectively.

Compositional Analysis. Compositional analysis was performed in a JEOL 3000F transmission electron microscope equipped with a field emission gun operated at 300 kV, a STEM unit, and an OXFORD energy-dispersive X-ray detector (silicon drift detector) plus the INCA analysis software. Nanowires were mechanically broken off from the substrate and transferred to a lacey carbon-covered copper grid for analysis.

Device Processing. After growth, nanowires were broken off from the growth substrate and transferred to a Si substrate capped with a 100 nm thick thermal oxide for device fabrication. Ohmic contacts to the InAs leads were defined using electron beam lithography, thermal evaporation of 25 nm Ni and 75 nm Au, and lift-off. Prior to metallization, an ammonium polysulfide ($(NH_4)_2S_x$) solution was used to strip the native oxide from the lithographically exposed InAs leads and to passivate the surface, protecting it from reoxidation.[23] On selected devices, two contacts were placed on each InAs lead in order to verify the Ohmic quality of the contacts using

DOI: 10.1021/acs.nanolett.5b04067
Nano Lett. 2016, 16, 1017−1021

four-probe measurements. The contacts were found to be Ohmic at all temperatures tested.

Simulations. Compositional data from the quantitative STEM−EDX analysis were used to construct a one-dimensional model of the potential structure along the length of the nanowire using a composition-weighted linear combination of InAs and InP material parameters to extrapolate corresponding parameters for the different ternary compositions of the steps. Current−voltage (I−V) characteristics were calculated numerically by solving Poisson's equation self-consistently coupled with equations for drift−diffusion current using a finite element method implemented in the semiconductor module of COMSOL Multiphysics 4.4. A detailed description of the simulations, including the model geometry and material parameters used, is provided in the Supporting Information.

■ ASSOCIATED CONTENT

Supporting Information

The Supporting Information is available free of charge on the ACS Publications website at DOI: 10.1021/acs.nanolett.5b04067.

TEM analysis of nanowire crystal structure and simulation details (PDF)

■ AUTHOR INFORMATION

Corresponding Author

*E-mail: lars.samuelson@ftf.lth.se.

Author Contributions

The manuscript was written through contributions of all authors. All authors have given approval to the final version of the manuscript.

Notes

The authors declare no competing financial interest.

■ ACKNOWLEDGMENTS

This work was performed within the NanoLund research center at Lund University, supported by the Knut and Alice Wallenberg Foundation (KAW), and was funded by grants from the Swedish Research Council (VR, grant no. 349-2008-6584 and grant no. 621-2011-4239).

■ REFERENCES

(1) Kroemer, H. *Proc. IEEE* **1963**, *51*, 1782−1783.
(2) Faist, J.; Capasso, F.; Sivco, D. L.; Sirtori, C.; Hutchinson, A. L.; Cho, A. Y. *Science* **1994**, *264*, 553−556.
(3) Mimura, T.; Hiyamizu, S.; Fujii, T.; Nanbu, K. *Jpn. J. Appl. Phys.* **1980**, *19*, L225−L227.
(4) Chang, L. L.; Esaki, L.; Tsu, R. *Appl. Phys. Lett.* **1974**, *24*, 593−595.
(5) Kroemer, H. *RCA Rev.* **1957**, *18*, 332−342.
(6) Capasso, F. *J. Vac. Sci. Technol., B: Microelectron. Process. Phenom.* **1983**, *1*, 457−461.
(7) Glas, F. *Phys. Rev. B: Condens. Matter Mater. Phys.* **2006**, *74*, 2−5.
(8) Ertekin, E.; Greaney, P. A.; Chrzan, D. C.; Sands, T. D. *J. Appl. Phys.* **2005**, *97*, 114325−10.
(9) de la Mata, M.; Magén, C.; Caroff, P.; Arbiol, J. *Nano Lett.* **2014**, *14*, 6614−6620.
(10) Björk, M. T.; Ohlsson, B. J.; Sass, T.; Persson, A. I.; Thelander, C.; Magnusson, M. H.; Deppert, K.; Wallenberg, L. R.; Samuelson, L. *Nano Lett.* **2002**, *2*, 87−89.
(11) Gudiksen, M. S.; Lauhon, L. J.; Wang, J.; Smith, D. C.; Lieber, C. M. *Nature* **2002**, *415*, 617−620.
(12) Wu, Y.; Fan, R.; Yang, P. *Nano Lett.* **2002**, *2*, 83−86.
(13) Thelander, C.; Mårtensson, T.; Björk, M. T.; Ohlsson, B. J.; Larsson, M. W.; Wallenberg, L. R.; Samuelson, L. *Appl. Phys. Lett.* **2003**, *83*, 2052−2054.
(14) Björk, M. T.; Ohlsson, B. J.; Thelander, C.; Persson, A. I.; Deppert, K.; Wallenberg, L. R.; Samuelson, L. *Appl. Phys. Lett.* **2002**, *81*, 4458−4460.
(15) Persson, A. I.; Björk, M. T.; Jeppesen, S.; Wagner, J. B.; Wallenberg, L. R.; Samuelson, L. *Nano Lett.* **2006**, *6*, 403−407.
(16) Trägårdh, J.; Persson, A. I.; Wagner, J. B.; Hessman, D.; Samuelson, L. *J. Appl. Phys.* **2007**, *101*, 123701−123704.
(17) Ohlsson, B. J.; Björk, M. T.; Magnusson, M. H.; Deppert, K.; Samuelson, L.; Wallenberg, L. R. *Appl. Phys. Lett.* **2001**, *79*, 3335−3337.
(18) Thelander, C.; Björk, M. T.; Larsson, M. W.; Hansen, A. E.; Wallenberg, L. R.; Samuelson, L. *Solid State Commun.* **2004**, *131*, 573−579.
(19) Mead, C.; Spitzer, W. *Phys. Rev. Lett.* **1963**, *10*, 471−472.
(20) Bhargava, S.; Blank, H.-R.; Narayanamurti, V.; Kroemer, H. *Appl. Phys. Lett.* **1997**, *70*, 759−761.
(21) Heiblum, M.; Nathan, M. I.; Thomas, D. C.; Knoedler, C. M. *Phys. Rev. Lett.* **1985**, *55*, 2200−2203.
(22) Williams, G. F.; Capasso, F.; Tsang, W. T. *IEEE Electron Device Lett.* **1982**, *3*, 71−73.
(23) Suyatin, D. B.; Thelander, C.; Björk, M. T.; Maximov, I.; Samuelson, L. *Nanotechnology* **2007**, *18*, 105307−5.

DOI: 10.1021/acs.nanolett.5b04067
Nano Lett. 2016, 16, 1017−1021